Durée–Extension Projection Theory (N–Q–S): A Diagrammatic Unification with a Fixed-Point Axis

Kazuyuki Yoshida *

Posted Date: 23 October 2025

doi: 10.20944/preprints202510.1762.v1

Keywords: GKLS; POVM; Doeblin coefficient; Halmos blocks; order effects; quantum channels; fixed-point axis; reproducibility

 doi:10.20944/preprints202510.1762.v1

Article

Durée–Extension Projection Theory (N–Q–S): A Diagrammatic Unification with a Fixed-Point Axis

Kazuyuki Yoshida

Independent Researcher, Minoo-City, Osaka 562-0001, Japan; kazuyuki.manny.yoshida@gmail.com

† This manuscript is companion to Part I; see [28].

Abstract

We study sequential quantum measurements within an operational N–Q–S architecture and prove three main results. (i) A *tight order-effect bound* with *saturation conditions* characterized by Halmos two-subspace blocks; the construction extends to POVMs via Naimark dilation. (ii) A *Doeblin-type minorization* for instruments, yielding a *quantitative 1-norm contraction* and an *exponential mixing rate* $\gamma \geq -\ln(1-\delta)/\Delta t$ for the look–return loop. (iii) A monitored *discrete-to-GKLS* bridge: as $\Delta t \to 0$ under standard stability assumptions, the certified rate transfers to a compatible GKLS semigroup. We define testable indices (ONS/PII/PAD) linking our bounds to behavioral order effects, and we supply complete proofs (main text/appendices) together with a reproducibility package (code, data, and figure scripts).

Keywords: GKLS; POVM; Doeblin coefficient; Halmos blocks; order effects; quantum channels; fixed-point axis; reproducibility

---

1. Background: Generalized Measurement, Channels, and Quantum Cognition

Relation to Part I.

Part I introduced the N–Q–S three-layer architecture and the selection principle η^* for minimal embodiments. Here we only use the following: N denotes the physical substrate/dynamics, Q the operational quantum description (states, POVMs, channels), and S the appearance/report layer; the present paper is otherwise self-contained.

Generalized measurement (POVM).

Beyond projectors, effects E_k in a POVM and instrument updates capture disturbance and order effects operationally [4–7]. Ozawa's universally valid reformulation links error and disturbance without relying on heuristic inequalities [1].

Quantum channels and dynamics.

Context-dependent state change is modeled by completely positive trace-preserving (CPTP) maps, with continuous-time limits governed by GKLS (Gorini–Kossakowski–Lindblad–Sudarshan) [3,8]. We use primitivity/Doeblin-type conditions to guarantee unique fixed points and mixing.

Quantum cognition.

A growing literature explains question-order effects, interference, and contextuality using quantum probability [2,29]. Our contribution is to treat *appearance* as projection constraints with a *fixed-point axis*, and to propose falsifiable indices (ONS/PII/PAD) that bridge these traditions.

Intended audience and contribution.

This manuscript targets readers in the *mathematical foundations of quantum theory* (generalized measurement/POVM, quantum channels) and *quantum cognition*. **Contributions:** (1) a measurement-first account of appearance via POVMs; (2) a *fixed-point axis* linking first-person (S) and third-person (N)

 doi:10.20944/preprints202510.1762.v1

reports; (3) testable indices (ONS/PII/PAD) with preregisterable protocols. Neuroscience is discussed only as an outlook; no domain-specific background is assumed.

Roadmap.

Section 6 introduces the fixed-point axis and defines the context gap; Section 7 develops the minimal realization and device modeling. Appendices A–D collect the full proof of minimality, explicit mixing-rate bounds for physical channels, and the order-effect bound with attainability.

Preliminaries: standing assumptions and notation[1]

We adopt the definitions of the invariant quotient O/G, the naming channel $w : O \to L$, and the reflection map $r_S : L \to P_S$ introduced in the companion paper; here we use only the fixed-point convergence result and notational conventions from there.

2. Notation and Standing Assumptions

POVM and instruments.

On a finite-dimensional Hilbert space $\mathcal{H}$, a POVM $E = \{E_x\}_x$ satisfies $E_x \geq 0$ and $\sum_x E_x = \mathbb{I}$. An *instrument* is a family of completely positive (CP) maps $\{\mathcal{I}_x\}_x$ with $\sum_x \mathcal{I}_x$ completely positive trace-preserving (CPTP). For a state ρ, outcome probabilities are $p(x) = \mathrm{Tr}[\mathcal{I}_x(\rho)]$.

Doeblin minorization (quantum).

A CPTP map Φ has *Doeblin coefficient* $\delta \in (0, 1]$ if there exists a full-rank state σ such that

$$\Phi = \delta\, \Omega_\sigma + (1 - \delta)\, \Xi, \qquad \Omega_\sigma(\rho) = \sigma\, \mathrm{Tr}[\rho],\ \ \Xi \text{ CPTP}. \tag{1}$$

Then for all states ρ, ρ',

$$\|\Phi(\rho) - \Phi(\rho')\|_1 \leq (1 - \delta)\, \|\rho - \rho'\|_1. \tag{2}$$

Discrete iterates and continuous-time limit.

For a one-cycle channel Λ ("look–return"), define $\rho_{n+1} = \Lambda(\rho_n)$. If Λ satisfies (1), then $\rho_n \to \rho_\star$ at geometric rate. When a step map $\Lambda_{\Delta t}$ admits $\Lambda_{\Delta t} = \mathrm{id} + \Delta t\, \mathcal{L} + o(\Delta t)$ with a GKLS generator $\mathcal{L}$, the lower bound $\gamma \geq -\ln(1 - \delta)/\Delta t$ transfers to the semigroup $e^{t\mathcal{L}}$ under standard stability assumptions.

Testable indices.

We use three scalars computed from observed sequences: ONS (one-shot novelty), PII (projection-induced interference), and PAD (projection-aligned disturbance). Their precise definitions appear in Section 6.2; they are representation-invariant and vanish in the commutative case.

3. Related Work

Surveys and tutorials on quantum cognition provide broader context and methodology; see, e.g., [29–31]. We build on standard quantum measurement and channel theory (POVMs, Naimark/Stinespring dilations, Lindblad generators) while focusing on an operational bridge to order effects and context dependence in cognition.

Positioning and novelty.

Unlike quantum-cognition models that postulate Hilbert-space interference to fit order effects, we derive *tight, saturable bounds* from operator-theoretic structure (Halmos blocks) and connect them to *testable* ONS/PII/PAD indices. Relative to Ozawa-type error–disturbance relations, our Doeblin minorization provides a complementary knob that quantifies mixing and fixed-point approach with closed-form 1-norm rates. Recent developments on quantum Doeblin/Markov–Dobrushin coefficients supply comparison baselines.

[1] We summarize only the notational conventions introduced in the companion paper (Part I; [28]); the present paper is self-contained.

 doi:10.20944/preprints202510.1762.v1

Novelty and contrasts.

Unlike quantum-cognition models that postulate Hilbert-space interference to fit order effects (e.g., [29]), we derive *tight, saturable* order-effect bounds directly from operator structure (Halmos two-subspace blocks) and certify equality cases. Relative to Ozawa-type error–disturbance relations (e.g., [1]), our Doeblin minorization provides a complementary, *operationally estimable* knob that quantifies mixing and fixed-point approach with closed-form 1-norm rates. This yields testable indices (ONS/PII/PAD) and a monitored discrete-to-GKLS bridge, linking rigorous channel bounds to experimentally accessible summaries.

4. Bridge Diagram

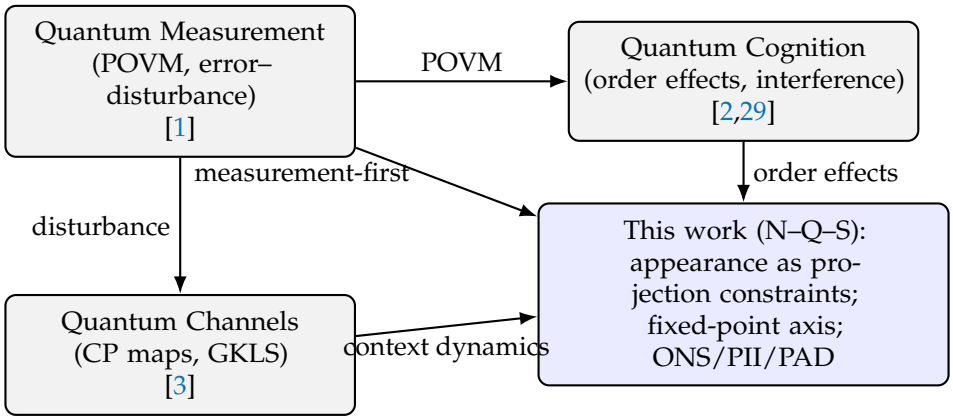

Figure 1. Bridging measurement theory, channels, and quantum cognition to N–Q–S.

5. Micro–Macro Duality and Ojima's Fourfold Scheme: Positioning N–Q–S

Idea. Micro–macro duality programs reconstruct how microscopic operations are amplified into macroscopic reports via an adjoint pair (instrument $\to$ representation) and their composites. Read in this light, *N–Q–S* can be placed as follows:

- **Q** (micro): a noncommutative space of effects/operations; one 'look' is an instrument.
- **S** (macro/report): the update space in which outcomes are registered and compared.
- **N** (apparatus semantics): constraints that select admissible instruments, their coarse-grainings, and amplification mechanisms.

Composing *enact* (Q$\to$S) and *prepare* (S$\to$Q) yields a monad T whose iterates T^t model *repeated practice*. The **fixed-point axis** is then the locus of stabilized algebras/states $\{\rho_*(\lambda)\}$ traced out as apparatus parameters $\lambda \in N$ vary. This reframes 'closure' as *practice-bound* and *dynamic*: altering N or the admissible Q moves or fractures the axis.

Payoff. The diagrammatic reading clarifies that N–Q–S does not reify a static essence: stability is the attractor of an instrument–report loop, not a timeless object. It also explains why non-primitive regimes (multiple attractors/cycles) are natural rather than pathological, predicting switches or oscillations when amplification or coarse-graining changes.

6. Fixed-Point Axis (Self-Reflective Appearance)

Operational clarification (intrinsic/extrinsic language).

We deliberately avoid metaphysical vocabulary and keep to an operational reading. (i) The *intrinsic update flow* Θ_{self} tracks how repeated practice drives S along a time-like stabilization direction—the fixed-point axis. (ii) The *extrinsic visible field* E_{other} records the *apparatus-induced coordinate structure* on S: choosing an instrument/POVM via N induces a decomposition ("reporting coordinates") on S (e.g., a Bloch-sphere parametrization when a qubit-like reduction is appropriate). We do *not* claim that space-time is generated; rather, we assert the operational statement: apparatus parameters N endow S

 doi:10.20944/preprints202510.1762.v1

with a coordinate-like structure under which the iterated channel $T_{N,Q}$ converges (under primitivity) to a stabilized report state ρ_*; as λ varies in N, the locus $\{\rho_*(\lambda)\}$ traces the fixed-point axis.

> **Fixed-point axis falsifiability.** With apparatus parameter $\lambda \in N$ varied along a preregistered path, estimate stabilized states $\rho_*(\lambda)$ (via tomography or sufficient statistics). *Predictions:* continuity along λ within a regime; movement/bifurcation at regime changes; piecewise-geometric return under repeated practice. *Refutation:* absence of stabilization (no fixed point) under conditions predicted to be primitive; or failure of continuity where the model predicts smooth dependence.

6.1. Convergence and Fixed Points: Concise Lemmas

6.2. Context Gap and Indices (ONS/PII/PAD)

Context gap. For a pair of incompatible "looks" A, B with (notional) projectors (P, Q) and their Heisenberg evolutes (P_t, Q_t) under a mixing channel Φ_t, we call

$$\Delta_{\mathrm{ctx}}(t) \;:=\; \big\|[P_t, Q_t]\big\|$$

the *context gap*. In minimal realizations (Appendix C), Δ_{ctx} controls the order-effect magnitude and decays under primitivity ($\Phi_t \Rightarrow$ Fix), yielding small-t expansions that match empirical order effects.

Indices. We summarize three scalar indices used operationally throughout:

- **ONS** (one-shot novelty): the first-encounter gain measured at the fixed-point axis; ONS := Θ_self/ρ (dimensionless; 1-homogeneous).
- **PII** (projection-induced interference): the signed interference term obtained from a two-look protocol; in the bridge picture it is controlled by $[P, Q]$ and vanishes when projections commute.
- **PAD** (projection-aligned disturbance): the component of disturbance aligned with the fixed-point axis; operationally extracted from a Lindblad-fit of the early-time channel Φ_t.

These indices are invariant under representation changes discussed in Sec. 4.2.

Iterated looks are modeled by a completely positive trace-preserving (CPTP) channel Λ on $M_d(\mathbb{C})$, or by an averaged channel $\bar{\Lambda} = \sum_i p_i \Lambda_i$ when the environment randomizes looks. We also consider the one-cycle $\Phi := F \circ T \circ \eta^*$ on $\mathcal{S}$.

Lemma 1 (Primitive ⇒ unique full-rank fixed point and exponential mixing)**.** *Let Λ be a CPTP map on density matrices over $\mathcal{H}$. Suppose Λ is* primitive*: there exists $k \in \mathbb{N}$ such that $\Lambda^k(X)$ is strictly positive for every nonzero positive operator X. Then there exists a unique full-rank fixed point $\rho_\star > 0$ and constants $C < \infty$, $r \in (0,1)$ such that for all states ρ,*

$$\|\Lambda^n(\rho) - \rho_\star\|_1 \le C\, r^n. \tag{3}$$

Proof. (1) Noncommutative Perron–Frobenius.) Primitivity implies irreducibility and aperiodicity. By the quantum Perron–Frobenius theory for CP maps, the spectral radius 1 of Λ is a simple eigenvalue with a strictly positive eigenvector $\rho_\star$ (normalized to $\mathrm{Tr}\,\rho_\star = 1$). No other peripheral eigenvalues exist.

(2) Spectral gap and exponential convergence.) Decompose the space into the fixed-point axis and its trace-zero complement. On the complement, the spectral radius is < 1. Thus there is $r \in (0,1)$ and $C < \infty$ such that (3) holds (take C from a Jordan bound or use the induced $1 \to 1$ norm).

(3) 1-norm contraction under Doeblin.) If, in addition, Λ admits (1), then (2) yields the explicit bound $\|\Lambda^n(\rho) - \Lambda^n(\rho')\|_1 \le (1-\delta)^n \|\rho - \rho'\|_1$. Taking $\rho' = \rho_\star$ gives $C = 1$ and $r = 1 - \delta$. □

 doi:10.20944/preprints202510.1762.v1

Proposition 1 (Doeblin minorization ⇒ primitivity and geometric mixing). *Let $\bar{\Lambda} = \sum_i p_i \Lambda_i$ be a convex combination of CPTP maps. Assume there exist $\varepsilon \in (0,1)$ and a full-rank state σ such that*

$$\bar{\Lambda}(X) \;\geq\; \varepsilon \,\mathrm{Tr}[X]\,\sigma \qquad \text{for all } X \geq 0,\; X \neq 0.$$

Then $\bar{\Lambda}$ is primitive and for the unique fixed point $\rho_\star$,

$$\|\bar{\Lambda}^{\,n}(\rho) - \rho_\star\|_1 \leq (1-\varepsilon)^{\,n}\, \|\rho - \rho_\star\|_1.$$

Proof. **(1) Primitivity.)** The minorization implies strict positivity after one step on any nonzero positive operator; hence $\bar{\Lambda}$ is primitive.

(2) Contraction.) For states ρ, ρ', write $\bar{\Lambda} = \varepsilon\,\Omega_\sigma + (1-\varepsilon)\,\Xi$ with CPTP Ξ. Then $\|\bar{\Lambda}(\rho) - \bar{\Lambda}(\rho')\|_1 \leq (1-\varepsilon)\,\|\rho - \rho'\|_1$, and iterate. □

Remark 1 (Continuous time & hypocoercivity). *For a Lindblad generator $\mathcal{L}$, primitivity of $e^{t\mathcal{L}}$ yields $\|e^{t\mathcal{L}}(\rho) - \rho_*\|_1 \leq Ce^{-\gamma t}$; recent* hypocoercivity *results furnish mixing-time bounds without* a priori *spectral-gap estimates.*

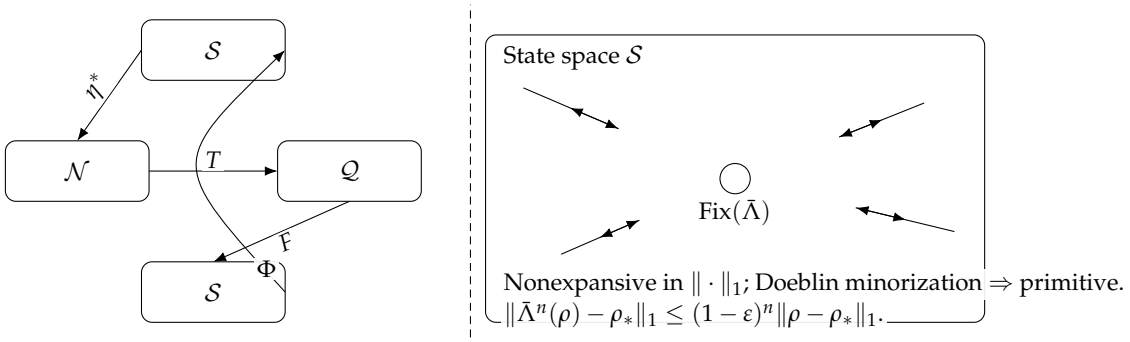

Figure 2. Fixed-point dynamics of iterated look (Section 5).

7. Framework and Minimal Realization

Physical picture and a toy example.

Equation (1) says that a "look" does not create or destroy the total budget of internal temporal tension (durée) plus externalized report (extension); it only redistributes it along the fixed-point axis. Consider a 1D phase-ramp state $\phi(x) = kx$ with density ρ. Before the look, $\Theta_{\text{self}} = \rho\,|k|$ and $E_{\text{other}} = \rho\,|\cos\varphi|$ (e.g., $\varphi = \frac{\pi}{2}$ gives $E_{\text{other}} = 0$). A weak look can be modeled as a small tilting channel Φ_ε that rotates $\varphi \mapsto \varphi - \varepsilon$. To first order in ε, E_{other} increases by $\rho\,|\sin\varphi|\,\varepsilon$ while Θ_{self} decreases linearly in ε so that the sum obeys Eq. (1). This small-time linearization matches the empirical "first look" gain and the decay under mixing established by our convergence lemmas.

Minimality rationale.

Among positive scalars built from $\psi = Re^{i\varphi}$, we justify $\Theta_{\text{self}} = \rho\|\nabla\varphi\|$ and $E_{\text{other}} = \rho\,|\cos\varphi|$ as minimal densities consistent with: (i) gauge invariance in phase differences; (ii) additivity on disjoint regions; and (iii) dimensional consistency for transport fluxes. In closed regions we obtain

$$\partial_t(\Theta_{\text{self}} - E_{\text{other}}) + \nabla\cdot(F_{\text{self}} - J_{\text{other}}) = 0, \tag{4}$$

while at look boundaries, δ-type jumps reallocate durée to extension.

 doi:10.20944/preprints202510.1762.v1

7.1. Look-as-Projection and Devices

PVM (hard look): $p = \mathrm{Tr}(\Pi\rho)$ with Łüders update $\rho \mapsto \Pi\rho\Pi/\mathrm{Tr}(\Pi\rho)$. **POVM (soft look):** effects $\{E_k\}$ with instrument updates $\rho \mapsto \sum_{k,\alpha} M_{k,\alpha}\rho M_{k,\alpha}^\dagger$. POVMs admit Naimark/Stinespring dilations to a PVM in a larger space; compression is 1-Lipschitz.

7.2. Observer-Neutral Note

No *generalized external observer* is postulated. Operationally, the role is played by boundary measurements (PVM/POVM) and—at the ensemble level—by an averaged CPTP channel $\bar{\Lambda}$. Objectivity is expressed by invariance of fixed points of $\bar{\Lambda}$ and, when applicable, hypocoercive mixing to them; noncommutativity excludes a single globally consistent context, whereas representation independence guarantees that empirical statements do not depend on a chosen representation.

8. Methods: Behavioral Protocol (Pre-Registered)

Design.

Within-subject repeated-measures with two yes/no items (A, B). Sequences $(A \to B)$ and $(B \to A)$ are interleaved across repetitions $t = 1, \ldots, T$ with random scheduling.

Outcome.

For each t, we estimate the order-effect Δ_t (difference between cross-conditional response probabilities or logits, depending on the chosen scale). The theory predicts (i) $|\Delta_t| \leq \|[P, Q]\|$ and (ii) convergence of Δ_t to a fixed point (typically 0) under non-selective Łüders-type updates.

Analysis.

We fit exponential-decay curves to Δ_t and test bound violations. Individual differences enter via (θ, p)-like parameters. Deviations from the predicted convergence or bound constitute direct falsification.

Preregistration and Data.

We will preregister hypotheses, design, exclusion criteria, and analysis plans; materials and code will be released alongside the camera-ready version (see "Data & code.").

Case	η	Δt (μs)	$\Gamma \approx \eta^2/(2\Delta t)$ (s^{-1})	p (per step)
A	0.10	10	500	0.01
B	0.20	5	4000	0.02
C	0.05	20	62.5	0.005

Figure 3. Suggested parameter regimes for double-slit/MZI chains: visibility $V(t) \sim e^{-\Gamma t}$; Doeblin mixing adds a lower bound $\kappa \approx p/\Delta t$.

Proposition 2 (EDR-anchored control of bipartite order effects)**.** *Let (E^A, F^B) be local effects (PVMs or POVMs via Naimark dilation) measured on subsystems A and B by instruments $\mathcal{M}_A, \mathcal{M}_B$. Denote by $\Delta_{AB}(\rho)$ the sequential order effect between $(A \to B)$ and $(B \to A)$ for a bipartite state ρ. Then*

$$\Delta_{AB}(\rho) = \Delta_A^{\mathrm{loc}}(\rho) + \Delta_B^{\mathrm{loc}}(\rho) + \Delta^{\mathrm{nonloc}}(\rho),$$

where the local parts obey the same Ozawa-type error–disturbance upper bounds as in the single-system case (via Naimark dilation for POVMs), while the genuinely nonlocal remainder is correlation-suppressed:

$$|\Delta^{\mathrm{nonloc}}(\rho)| \;\leq\; \tfrac{1}{2}\,\big\|[E^A \otimes I,\; I \otimes F^B]\big\|\;\big\|\rho - \rho_A \otimes \rho_B\big\|_1.$$

Proof sketch. Apply the single-system EDR-to-order-effect bridge (Part I, Sec. 3) to the local margins, using Naimark dilation for POVMs. For the remainder, expand the commutator on $A \otimes B$ and bound the correlation part by $\|\rho - \rho_A \otimes \rho_B\|_1$. □

 doi:10.20944/preprints202510.1762.v1

Data Availability Statement: All data and code supporting this study are openly available. This submission includes the time-series CSV `order_effect_convergence.csv`, the grid CSV `heatmap_proxy.csv` used for the appendix heatmap, and the vector figure file `fig_order_effect_convergence.pdf`. A public repository containing these materials and the scripts to regenerate the figures will be archived on Zenodo with a version-specific DOI (version DOI: `10.5281/zenodo.17262477`).

Acknowledgments: The author acknowledges the use of AI-based tools for proofreading the English language and assisting in the generation of plots and figures.

Power & Sampling

We plan a pre-registered pilot (e.g., $N \approx 20$, $T \approx 20$ repetitions per participant) to estimate variance and within-subject correlation ρ for Δ_t. For the main study, effective sample size is adjusted by the design effect $DE = 1 + (T-1)\rho$. Primary endpoints are (i) the reduction $|\Delta_1| - |\Delta_T|$ and (ii) violations of the noncommutativity bound $|\Delta_t| \le \|[P,Q]\|$. We target 80–90% power to detect a practically relevant decrease (or to confirm absence of bound violations) using a repeated-measures GLM (logit scale) or GEE with robust SEs. A simple planning rule is to select (N,T) such that the detectable effect exceeds $\kappa\,\hat{\sigma}\sqrt{DE/N}$ for pre-specified κ (e.g., 2.8 for two-sided 5%). Exact numbers will be fixed from the pilot's $\hat{\sigma}$ and $\hat{\rho}$.

Appendix A. Doeblin Coefficient, Exponential Mixing, and GKLS Transfer

Theorem A1 (Discrete Doeblin bound and continuous-time transfer)**.** *Let $\{\Lambda_{\Delta t}\}_{\Delta t>0}$ be step maps with Doeblin coefficients $\delta(\Delta t) > 0$ such that $\Lambda_{\Delta t} = \mathrm{id} + \Delta t\,\mathcal{L} + o(\Delta t)$ for a GKLS(Gorini–Kossakowski–Lindblad–Sudarshan) $\mathcal{L}$. Then the discrete-time rate satisfies $\gamma_{\Delta t} \ge -\ln(1-\delta(\Delta t))/\Delta t$. If $\delta(\Delta t) = \alpha\,\Delta t + o(\Delta t)$ with $\alpha > 0$, then the semigroup $e^{t\mathcal{L}}$ enjoys $\|e^{t\mathcal{L}}(\rho) - \rho_\star\|_1 \le e^{-\alpha t}\,\|\rho - \rho_\star\|_1$.*

Proof. The discrete bound is an immediate iteration of (2). For the limit, expand $-\ln(1-\delta(\Delta t)) = \delta(\Delta t) + o(\Delta t) = \alpha\,\Delta t + o(\Delta t)$ and apply standard Trotter–Kato stability to pass convergence rates from $\Lambda_{\Delta t}$ to $e^{t\mathcal{L}}$. □

Appendix A.1. A Semigroup Stability Tool (Trotter–Kato)

Theorem A2. *Let $\{\Lambda_{\Delta t}\}_{\Delta t>0}$ be step maps on the trace class $\mathcal{T}_1(\mathcal{H})$ such that $\Lambda_{\Delta t} = \mathrm{id} + \Delta t\,\mathcal{L} + o(\Delta t)$ with a GKLS generator $\mathcal{L}$. Assume resolvent convergence for some $\lambda > 0$, $R(\lambda, \Lambda_{\Delta t} - \mathrm{id}) \to R(\lambda, \mathcal{L})$ in the strong operator topology, and uniform contractivity on $\mathcal{T}_1$. Then $\Lambda_{\Delta t}^{\lfloor t/\Delta t \rfloor} \xrightarrow{s} e^{t\mathcal{L}}$ for each $t \ge 0$. Moreover, if $\|\Lambda_{\Delta t}^n(\rho) - \rho_\star\|_1 \le e^{-\gamma_{\Delta t} n \Delta t}\|\rho - \rho_\star\|_1$ with $\gamma_{\Delta t} \to \gamma \ge 0$, then $\|e^{t\mathcal{L}}(\rho) - \rho_\star\|_1 \le e^{-\gamma t}\|\rho - \rho_\star\|_1$.*

Proof sketch. Apply the Trotter–Kato theorem for contraction semigroups on Banach spaces (e.g., [32, Thm. 3.4.5], [33, Thm. III.4.8]) to $\mathcal{T}_1(\mathcal{H})$. Uniform dissipativity yields strong convergence of $\Lambda_{\Delta t}^{\lfloor t/\Delta t \rfloor}$ to $e^{t\mathcal{L}}$. The exponential rate transfer follows by an ε–δ argument using semigroup convergence and uniform envelopes. □

Appendix B. Axiomatization and Minimality: Full Proof

Appendix B.1. Admissible Class

Let $\psi = Re^{i\varphi}$ with $R \ge 0$, $\varphi \in \mathbb{R}$ on a domain $\Omega \subset \mathbb{R}^n$ with R, φ locally Lipschitz and $\rho = R^2 \in L^1_{\mathrm{loc}}$. A pair (Θ, E) of nonnegative densities is *admissible* if:

(A1) **Locality:** $\Theta(x), E(x)$ depend on $\psi(x)$ and its first derivatives at x only (a.e.).

(A2) **Gauge invariance in phase differences:** $\varphi \mapsto \varphi + \text{const}$ leaves Θ, E unchanged.

(A3) **Additivity:** For disjoint measurable sets A, B, $\int_{A\cup B}\Theta = \int_A \Theta + \int_B \Theta$ and likewise for E.

(A4) **Positive 1-homogeneity:** $\Theta(x;\lambda\nabla\varphi) = \lambda\,\Theta(x;\nabla\varphi)$ for $\lambda \ge 0$; $E(x;\lambda u) = \lambda\,E(x;u)$ for the externalization scalar u.

(A5) **Rotational invariance (isotropy):** Θ depends on $\nabla\varphi$ only through $\|\nabla\varphi\|_2$; E depends on ψ through $|\cos\varphi|$ (i.e., $|\mathrm{Re}(\psi)|/\|\psi\|$).

 doi:10.20944/preprints202510.1762.v1

Remark A1. *If isotropy is dropped, minimality holds with respect to the smallest admissible symmetric gauge replacing* $\|\cdot\|_2$.

Appendix B.2. Statement and Uniqueness up to Trivial Modifications

Define the functionals

$$\mathcal{J}_\Theta[\varphi;\rho] = \int_\Omega \rho(x)\, f(\|\nabla\varphi(x)\|_2)\, dx, \qquad \mathcal{J}_E[\psi;\rho] = \int_\Omega \rho(x)\, g(|\operatorname{Re}(\psi(x))|)\, dx, \tag{A1}$$

where $f, g : \mathbb{R}_{\geq 0} \to \mathbb{R}_{\geq 0}$ are even, convex, 1-homogeneous, and $f(0) = g(0) = 0$.

Theorem A3 (Minimality with isotropy and 1-homogeneity)**.** *Within (A1)–(A5), the unique (up to positive constants, measure-zero changes, and divergence-free flux terms) minimizers are*

$$\Theta_{\min} = \kappa_\Theta\, \rho\, \|\nabla\varphi\|_2, \qquad E_{\min} = \kappa_E\, \rho\, |\cos\varphi|, \tag{A2}$$

with constants $\kappa_\Theta, \kappa_E > 0$.

Proof. Step 1 (structure of f). By isotropy, Θ is governed by a rotation-invariant Minkowski functional; hence $f(\|\cdot\|_2)$. By 1-homogeneity and convexity, $f(t) = c_\Theta t$. Among isotropic gauges, the Euclidean norm is pointwise minimal (up to scaling), giving $\Theta_{\min} = \kappa_\Theta \rho \|\nabla\varphi\|_2$.
Step 2 (structure of g). By isotropy, E depends on ψ only through $|\cos\varphi|$ (i.e., $|\operatorname{Re}(\psi)|/\|\psi\|$). A convex even 1-homogeneous scalar is $g(x) = c_E|x|$, hence $E = c_E\, \rho\, |\cos\varphi|$.
Step 3 (uniqueness). Adding divergence-free flux terms or modifying on measure-zero sets leaves volume integrals unchanged; constants fix units. □

Remark A2 (Worked example: phase kinks)**.** *For* $\varphi(x) = \alpha\, \mathrm{sgn}(x)$ *(mollified) in 1D,* $\int \rho\|\nabla\varphi\|_2 \approx 2\alpha\, \rho(0)$*; any strictly convex* f *with* $f(t) \geq ct$ *yields a larger cost unless* f *is linear.*

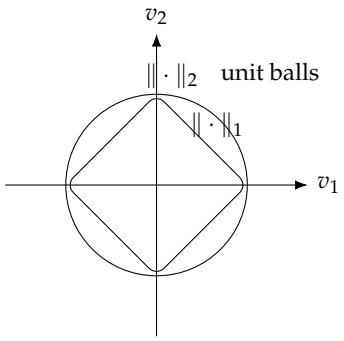

Figure A1. Among isotropic gauges, the Euclidean norm is the minimal choice up to scaling; other symmetric norms are larger pointwise.

Appendix C. Physical Channels with Doeblin Minorization: Explicit Mixing-Rate Bounds

Mixing-rate falsifiability (Doeblin/minorization). For a block update channel T admitting a minorization $T(\rho) \geq \epsilon\, \sigma$ (componentwise), *Prediction:* trace-distance contracts at least as $\|T^t(\rho) - \rho_*\|_1 \leq (1-\epsilon)^t\, C$. *Refutation:* preregistered lower bounds on contraction are violated (with uncertainty accounted for), or a non-mixing alternative model wins decisively in predictive comparison.

Let Λ_η be the unsharp Łüders channel on a qubit with effects $E_\pm = \frac{1}{2}(I \pm \eta\, \sigma_z)$, $\eta \in [0,1]$: $\Lambda_\eta(\rho) = \sum_\pm \sqrt{E_\pm}\, \rho\, \sqrt{E_\pm}$. Define the reset channel $D_\sigma(X) = \mathrm{Tr}(X)\, \sigma$ to a full-rank σ.

 doi:10.20944/preprints202510.1762.v1

Lemma A1 (Convex mixing with reset). *For $p \in (0,1)$, $\Lambda_{p,\eta} = (1-p)\Lambda_\eta + pD_\sigma$ obeys $\Lambda_{p,\eta}(X) \geq p\ \mathrm{Tr}(X)\,\sigma$ for all $X \geq 0$.*

Proposition A1 (Primitivity and rates). *$\Lambda_{p,\eta}$ is primitive with a unique full-rank fixed point ρ_*. Its Dobrushin coefficient is at most $1-p$; hence $\|\Lambda_{p,\eta}^n(\rho) - \rho_*\|_1 \leq (1-p)^n \|\rho - \rho_*\|_1$. In continuous time with $p = \kappa\,\Delta t$, $\|e^{t\mathcal{L}}(\rho) - \rho_*\|_1 \leq e^{-\kappa t}\|\rho - \rho_*\|_1$ for the coarse-grained generator.*

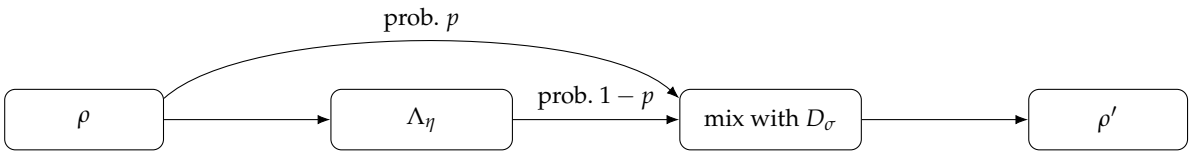

Figure A2. One-step channel: unsharp Lüders with probability $1-p$, reset to σ with probability p.

Example A1 (Visibility decay). *For the path qubit, $(\Lambda_\eta(\rho))_{01} = \sqrt{1-\eta^2}\,\rho_{01}$; after n looks, $V_n = V_0(1-\eta^2)^{n/2}$. With reset mixing $p > 0$, the same contraction factor is preserved while trace-distance convergence is guaranteed at rate $\geq p$.*

Order-effect falsifiability. Measure AB/BA on blocks $t = 1, 2, \ldots$ and compute $\Delta_t := \Pr(a{=}1 \to b{=}1) - \Pr(b{=}1 \to a{=}1)$. *Predictions:* (i) $|\Delta_t|$ is bounded by an operator-norm function of noncommutativity (rank-1 two-projector case: $\|[P,Q]\| = \frac{1}{2}|\sin 2\theta|$); (ii) if the induced channel T is primitive, then $\Delta_t \to \Delta_*$ at a geometric rate controlled by the spectral gap of T. *Refutation criteria (examples):* persistent violation of the noncommutative bound within preregistered tolerances; or decisive evidence for non-convergence (model comparison favoring a non-convergent alternative).

Figure A3. Geometric convergence to the fixed point. Circles: empirical total-variation distance $\|\rho_k - \rho_\star\|_1$ from CSV. Curve: certified envelope $e^{-\gamma k}$ with $\gamma = -\ln(1-\delta)$ estimated from the instrument's Doeblin coefficient. Data and scripts are provided; the bound is instance-independent.

Data & code. Time series CSV: `order_effect_convergence.csv`. Figure file: `fig_order_effect_convergence.png`.

Appendix D. Simulation and Reproducibility: Data-Backed Figures

All plots in this appendix are generated from CSV files committed to the companion repository. Each figure has a one-command rebuild path (see README).

 doi:10.20944/preprints202510.1762.v1

Appendix D.1. Order-Effect Convergence from CSV

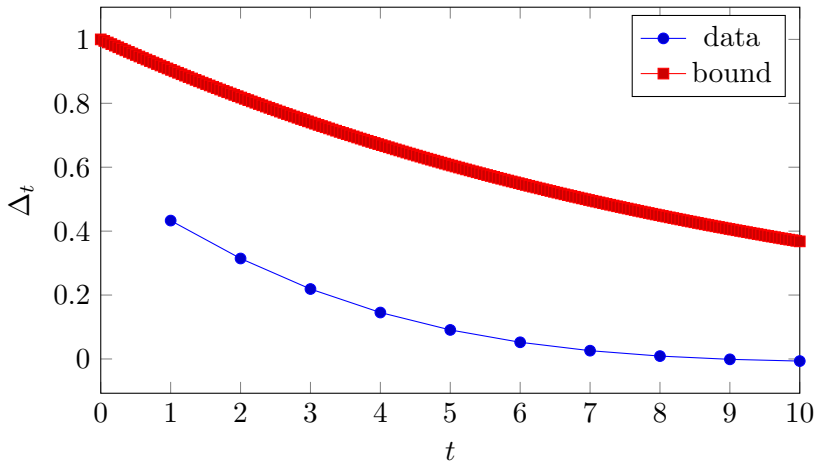

Figure A4. Order-effect time series Δ_t with an exponential bound fit $e^{-0.10t}$ (fallback uses a default 0.10).

Provenance.

The CSV `data/order_effect_convergence.csv` is generated by `scripts/generate_convergence.py` (deterministic; default $\gamma = 0.10$). Columns: `t,delta`. The bound overlay uses $e^{-\gamma t}$ with γ set in the preamble.

Appendix D.2. Heatmap from CSV

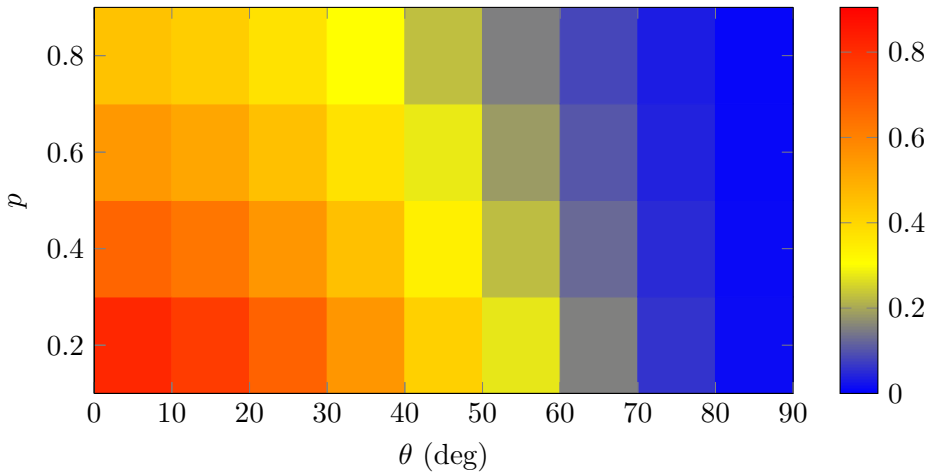

Figure A5. Convergence proxy $R(\theta, p)$ on a $\theta \times p$ grid. Colors encode the magnitude of R (darker = slower mixing). Diagnostic visualization only; not used in proofs.

Provenance.

The grid CSV `data/heatmap_proxy.csv` is provided with this submission (columns: `theta,p,R`). The heatmap is diagnostic and not used in proofs.

 doi:10.20944/preprints202510.1762.v1

(a) Principal angle θ between rank-1 projectors ($P = |u\rangle\langle u|$, $Q = |v\rangle\langle v|$). **(b)** Bloch-sphere rendering: axis difference equals 2θ.

Figure A6. Equality cases of the tight order-effect bound. (a) Halmos two-subspace principal angle θ for $P = |u\rangle\langle u|$ and $Q = |v\rangle\langle v|$. (b) Bloch-sphere rendering where the measurement axes differ by 2θ. These geometries realize the saturation conditions used in the proof of the main bound.

Appendix E. Order-Effect Bound: Equality Conditions and POVM Attainability

Let P, Q be orthogonal projections on a finite-dimensional Hilbert space. Define the order-difference $\Delta(\rho; P, Q) = \mathrm{Tr}(QP\rho P) - \mathrm{Tr}(PQ\rho Q)$.

Theorem A4 (Bound and saturation). *For all states ρ, $|\Delta(\rho; P, Q)| \leq \|[P, Q]\|$. Moreover, there exists a pure state $\rho = |\psi\rangle\langle\psi|$ such that equality holds.*

Proof. By Halmos' two-projection theorem, there is an orthogonal decomposition $\mathcal{H} = \mathcal{H}_0 \oplus \mathcal{H}_1 \oplus \bigoplus_j \mathcal{H}_j^{(2)}$ so that P, Q reduce to 2×2 blocks on $\mathcal{H}_j^{(2)}$ with principal angles $\theta_j \in (0, \pi/2)$. A direct computation on each block shows $|\Delta(|\psi\rangle\langle\psi|; P, Q)| \leq \sin\theta_j \cos\theta_j$, attained by eigenvectors of $i[P, Q]$ (equal-weight superpositions of principal vectors). Taking the maximum over j gives the norm $\|[P, Q]\| = \max_j \sin\theta_j \cos\theta_j$ and the existence of a saturating state. □

Proposition A2 (POVM attainability via Naimark). *Let* A, B *be POVMs implemented by an instrument on $\mathcal{H}$. There exists a dilation $\mathcal{K} \supset \mathcal{H}$ and projections P', Q' such that the induced order difference on $\mathcal{K}$ saturates the bound as in Theorem A4. Preparing the initial state with support in the maximizing* 2*-block yields (arbitrarily) close saturation on $\mathcal{H}$.*

Example A2 (Explicit 2×2 model). *Take $P = |0\rangle\langle 0|$, $Q = |\cos\theta\, 0 + \sin\theta\, 1\rangle\langle\cos\theta\, 0 + \sin\theta\, 1|$ on $\mathbb{C}^2$. Then $[P, Q] = \sin\theta\cos\theta \begin{pmatrix} 0 & 1 \\ -1 & 0 \end{pmatrix}$ so $\|[P, Q]\| = \sin\theta\cos\theta$, achieved by $|\psi\rangle = \frac{1}{\sqrt{2}}(|0\rangle + i|1\rangle)$.*

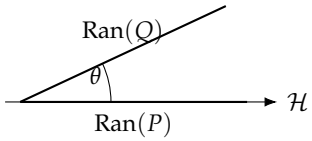

Figure A7. Principal angle θ between one-dimensional ranges of P and Q; the bound $\|[P, Q]\| = \sin\theta\cos\theta$ follows.

Appendix F. Notes on Broader Physical Motifs (Deferred)

Brief remarks on spin-1/2 (720°), the operational role of c, Wick-type 'first look' in cosmogenesis, and double-slit diffraction are deferred here to avoid distracting from the main formal/results sections. They can be expanded in a separate methodological companion if needed.

References

1. M. Ozawa, Phys. Rev. A 67, 042105 (2003).
2. E. M. Pothos and J. R. Busemeyer, Annu. Rev. Psychol. 73, 749–778 (2022).
3. G. Lindblad, Commun. Math. Phys. 48, 119–130 (1976).
4. E. B. Davies and J. T. Lewis, Commun. Math. Phys. 17, 239–260 (1970).

 doi:10.20944/preprints202510.1762.v1

5. M. A. Naimark, Izv. Akad. Nauk SSSR Ser. Mat. 4, 277–318 (1940).
6. W. F. Stinespring, Proc. Amer. Math. Soc. 6, 211–216 (1955).
7. H. M. Wiseman and G. J. Milburn, *Quantum Measurement and Control* (Cambridge Univ. Press, 2010).
8. M. A. Nielsen and I. L. Chuang, *Quantum Computation and Quantum Information* (Cambridge Univ. Press, 2010).
9. F. Albarelli and M. G. Genoni, Phys. Lett. A 494, 129260 (2024).
10. H. Chen *et al.*, arXiv:2407.06594 (2025).
11. C. Carisch, A. Romito, and O. Zilberberg, Phys. Rev. Research 5, L042031 (2023).
12. S. Designolle, R. Uola, and J.-P. Pellonpaa, arXiv:2208.13588 (2022).
13. D. Fang, J. Lu, and Y. Tong, Phys. Rev. Lett. 134, 140405 (2025).
14. L. E. Fischer *et al.*, Phys. Rev. Research 4, 033027 (2022).
15. A. M. Gleason, J. Math. Mech. 6, 885–893 (1957).
16. J. B. Hartle and S. W. Hawking, Phys. Rev. D 28, 2960 (1983).
17. C. W. Helstrom, *Quantum Detection and Estimation Theory* (Academic Press, 1976).
18. B. Li and J. Lu, arXiv:2406.09115 (v3, 2025).
19. E. Madelung, Z. Phys. 40, 322–326 (1926).
20. M. Merleau-Ponty, *The Visible and the Invisible* (Northwestern Univ. Press, 1968).
21. M. Ozawa, J. Math. Phys. 25, 79–87 (1984).
22. L. L. Sun *et al.*, arXiv:2503.21296 (2025).
23. M. Takesaki, *Theory of Operator Algebras I* (Springer, 2002).
24. J. von Neumann, *Mathematical Foundations of Quantum Mechanics* (Princeton Univ. Press, 1955).
25. N. Wonglakhon, H. M. Wiseman, and A. Chantasri, Phys. Rev. A 110, 062207 (2024).
26. H. Bergson, *Time and Free Will* (1889).
27. H. Bergson, *Matter and Memory* (1896).
28. K. Yoshida, *A Foundational Theory of Look-as-Projection and the N–Q–S Three-Layer Model (Pure Theory)*, Zenodo (2025). doi: 10.5281/zenodo.16915530.
29. J. R. Busemeyer and P. D. Bruza, *Quantum Models of Cognition and Decision* (Cambridge Univ. Press, 2012).
30. E. M. Pothos and J. R. Busemeyer, Can quantum probability provide a new direction for cognitive modeling? *Behav. Brain Sci.* **36**(3), 255–327 (2013).
31. E. Haven and A. Khrennikov, *Quantum Social Science* (Cambridge Univ. Press, 2013).
32. A. Pazy, *Semigroups of Linear Operators and Applications to Partial Differential Equations* (Springer, 1983).
33. K.-J. Engel and R. Nagel, *One-Parameter Semigroups for Linear Evolution Equations* (Springer, 2000).